The detective quantum efficiency of medical x-ray image intensifiers

J. T. Thirlwall[a)]
Division of Materials Science and Technology, Council for Scientific and Industrial Research, Pretoria, 0001, South Africa

(Received 30 April 1998; accepted for publication 18 August 1998)

The recognition of small features of low contrast in the image recorded by an x-ray image intensifier is usually limited by photon noise. This detail-contrast perceptibility is dependent on the detective quantum efficiency (DQE) and the modulation transfer function of the imaging tube and associated scanning system. The DQE can be calculated for all input photon energies from the statistical behavior of each stage of photon detection and amplification where quanta are lost or converted. The potential improvement to be obtained from any proposed design change can be estimated. The escape of characteristic photons from the input phosphor layer causes significant change to the performance particularly when gadolinium oxysulphide is employed for that purpose. © *1998 American Institute of Physics.* [S0034-6748(98)02511-8]

I. INTRODUCTION

The ability of an observer to perceive a small feature of low contrast with an x-ray image intensifier (XRII) has been shown to be dependent on the detective quantum efficiency (DQE) of the system and its modulation transfer function (MTF).[1] Although considerable attention has been paid to the instrument components which together determine the MTF,[2] the variation of DQE with incident photon energy is not often emphasized. Manufacturers of equipment for the medical field usually report the DQE of their products measured with Am^{241} as the photon source (59.57 keV), this being in the energy range of greatest efficiency; at other energies the DQE falls well below the ideal value of unity.

The DQE of a radioscopic system can be calculated for all photon energies from a knowledge of the structure of the image tube and the estimated or measured values of the quantum interaction at each stage of detection and amplification. This allows a better understanding of the performance characteristics of some radioscopic systems to be obtained, prediction of the results of any proposed structural change, and more accurate assessment of the detail-contrast perceptibility, or acuity, in their application to specific radiographic tasks.

II. MODELING THE XRII

The flux of x-ray photons entering a small area of the input window of the intensifier undergoes a sequence of attenuation, quantum conversions, and amplifications, each of which adds to the random nature of the quantum flux. As the signal passes through the structure the ratio of the integrated signal to its noise component, measured within a defined frequency range, inevitably decreases at every stage. A simple sequence of n secondary-electron stages of amplification was first modeled by Shockley and Pierce[3] in early studies of the cascade electron multiplier. They showed that the output noise N_{out} could be related to the noise of the input signal N_{in} by

$$N_{\text{out}}^2=(M.N_{\text{in}})^2(1+B), \tag{1}$$

where

$$B=b_1+\frac{b_2}{m_1}+\frac{b_3}{m_1.m_2}\ldots.+\frac{b_r}{m_1\ldots m_{r-1}}\ldots.. + \frac{b_n}{m_1\ldots m_{n-1}}, \tag{2}$$

where M is the overall system gain, B its relative variance, and m_r and b_r are the gain and relative variance of the rth stage. The model required that each quantum entering a stage had the same probability $p(g)$ of causing g quanta to emerge, that the quanta be independent (no space charge effects, for example), that the performance of each stage be independent of events in other stages, and that transit time variation be small compared with the period of the highest frequency in the recorded signal. The model was independent of the input noise characteristics.

Rose[4] and Clark Jones[5] introduced and developed the concept of the detective quantum efficiency as a measure of a detector's performance and, for the present purpose, it can be expressed in terms of the signal-to-noise ratio (SNR) at input and output of a real detector. From Eqs. (1) and (2) above

$$\text{DQE}=(\text{SNR})_{\text{out}}^2/(\text{SNR})_{\text{in}}^2=1/(1+B). \tag{3}$$

This model has been developed to describe the behavior of other devices including photon-scintillation detectors,[6] secondary-electron detectors,[7] and x-ray detectors.[8,9] These and the present work include processes in which the number of quanta is attenuated, stages which are not independent, and those in which $p(g)$ is not the same for all quanta. The variance of each stage, which is a measure of the spread of outputs obtained from a single quantum entering that stage, may be calculated on the basis that they are described by

a)Electronic mail: thirl@btinternet.com or Cc: thirl@iafrica.com

TABLE I. The gain and relative variance of each stage in the detection of a 30 keV photon using a CsI input phosphor. (Characteristic photon escape does not occur at this energy.)

Stage	Description	Gain	Relative variance
1	Penetration of primary photons through input window[a]	0.36	1.78
2	Partial absorption of x-ray flux in phosphor layer[a]	0.8	0.25
e	Characteristic photon escape from the phosphor	1	0
3	Generation of light photons in the phosphor[b]	1600	0.0006
4	Transmission of photons to the photoemissive layer[a]	0.5	1
5	Emission of photoelectrons[a]	0.1	9
	(The subsequent stages are omitted from this analysis.)		
		From Eq. (3):DQE=0.28	

[a]Binomial statistical model.
[b]Gaussian statistical model.

binomial or Gaussian probability statistics as appropriate or obtained by numerical methods. (The word variance hereafter refers to the relative variance of a process unless stated to the contrary.)

The DQE is estimated for a small area within the image, large in comparison with the ''spatial resolution'' of the XRII, and no account is taken of the well-known limitations on that resolution such as x-ray scatter by the input window and ''leakage'' of light photons across the face of the input phosphor layer which contribute to the MTF. The model is illustrated by calculating the DQE of XRII models with two types of input phosphor. Examples of the first have cesium iodide input phosphors 0.2 g/sq. cm (0.44 mm) and 0.1 g/sq. cm thick, grown from the vapor phase in columnar crystal form behind an input vacuum envelope of 4 mm glass with a 0.5 mm aluminum light-tight protective shield; another example has the thicker phosphor with a 0.25 mm titanium window.[10] The second type is assumed to have powder phosphor layers of gadolinium oxysulphide, Gd_2O_2S, 0.18 g/sq. cm (0.25 mm full density) and 0.09 g/sq. cm thick, each behind a 1.6 mm thick aluminum window.

The stages of an XRII relevant to this analysis are outlined in Table I. The monoenergetic x-ray signal is first attenuated by absorption and scatter during transmission through the input window. The ''gain'' m_1 of this stage will have a variance, from binomial statistical theory, of $b_1 = [m_1(1-m_1)/m_1^2]$. The signal is then similarly attenuated by incomplete absorption in the input phosphor layer (m_2, b_2). In the phosphor the detected signal is amplified by generating a large number of photons in the visible wavelength range. The gain m_3 has a variance $1/m_3$ as this stage, with high energy primary photons, is described by the Gaussian probability distribution. Following generation at a point within the phosphor, a fraction m_4 of the visible photons reaches the photoemissive layer at the rear face of the phosphor, the remainder being lost by scatter or self-absorption. A small fraction m_5 of the photon signal causes the emission of photoelectrons from that layer and these are accelerated through the electron-optical structure of the vacuum tube to strike the output phosphor. Photons from this second phosphor pass through the output window or channel plate to the recording or observation system. Table I lists as an example the gain and variance of the early stages of an XRII with an input signal of 30 keV photons. At this energy no escape events are possible and the DQE can be calculated from Eqs. (2) and (3).

Due to the large signal gain at the phosphor, particularly with high-energy photons, the variances of stages after the photoemitter have negligible influence on the value of B and these have been omitted from the calculations reported here. It has been pointed out, however,[11] that with an intense x-ray input, the XRII output signal may have to be attenuated, for example with an iris in the optical components, in order that the signal stays within the dynamic range of the recording device. In these circumstances it is possible that the additive noise power contributed by the recording device will dominate the attenuated noise of the XRII.

III. ESCAPE PROCESS

When the energy of a primary photon exceeds the K-shell excitation energy of any element in the phosphor, a characteristic $K\alpha$ or $K\beta$ photon can be generated by the fluorescence process. If this is not reabsorbed in the phosphor, less energy is deposited thus generating a smaller pulse of visible photons. For iodine this occurs above 33.17 keV and for cesium above 35.98 keV. This escape phenomenon can be regarded as an additional stage of which the gain m_e and variance b_e are estimated as outlined in the next section; the gain is the mean fraction of the primary photon energy which is deposited. The gain of the following stage, the generation of visible photons, however, now has a bimodal distribution with amplitudes determined by events in the escape stage. Breitenberger,[6] in considering the effects of a nonmonochromatic primary signal, has demonstrated that a dependant stage of this type can be included in the expression for total variance as

$$B = b_1 + \frac{b_2}{m_1} + \frac{b_e}{m_1.m_2} + \frac{b_3}{m_1.m_2.m_e} \cdots + \frac{b_n}{m_1 \ldots m_{n-1}.m_e}. \quad (4)$$

Although the algebraic form is identical to Eq. (2), the escape stage is fundamentally different in its origins. Equation (4) requires the gain and true variance of the following stage, m_3 and $(b_3.m_3^2)$, respectively, to be proportional to its input signal, that is the input energy here, a condition which

is satisfied for high-energy photons entering the phosphor where a large number of photons in the visible energy range is generated. The requirement, however, that all quanta have the same probability $p(g)$ of causing g quanta to be generated is not satisfied when the escape process can operate because the probability of characteristic photon escape changes with depth of origin in the phosphor layer; the probability of escape controls the mean fraction of the primary energy deposited in the phosphor. This can be modeled by considering the phosphor as t sublayers parallel to the surface. The gain $m_{e,s}$ and variance $b_{e,s}$ of each sublayer can be estimated and added, weighted in proportion to the probability of primary photon interaction $(m_{2,s}/m_2)$ in each sublayer, so that the total gain of the escape stage is

$$m_e = \sum [(m_{2,s} . m_{e,s})/m_2] \quad \text{for } s=1 \text{ to } t$$

and the total noise N is given by

$$N^2 = \sum [(m_{2,s} . m_{e,s}^2 . b_{e,s})/m_2]. \tag{5}$$

From these the variance of the escape stage is $b_e = N^2/m_e^2$.

IV. CALCULATION OF THE ESCAPE PROBABILITY

The mechanism of fluoresced photon escape in a phosphor generates light pulses containing, on average, fewer photons to a degree determined by the energies of the primary and escaped quanta. The mean and variance of the photon spectrum is obtained from this data and from the probability of an escape event.

The probability of generating a characteristic $K\alpha/\beta$ photon from Cs or I following a primary interaction of sufficient energy is determined by three factors: the probability of interaction of the primary radiation with Cs and I atoms; the probability that the atom will have K- rather than L- or M-shell excitation which is given by the K-edge ''jump ratio'';[12] the probability that K-shell excitation will generate a $K\alpha/\beta$ photon (and not undergo an Auger interaction) which is given by the fluorescent yield.[13] (For the purposes of this work the lower intensity $K\beta$ emission is treated as part of the $K\alpha$ emission). Following Reed and Ware,[14] the probability p_B of backward escape from a thick phosphor is obtained by integration through the semi-infinite thickness and over all directions of emission so that

$$p_B = 0.5Q\{1-(\mu'/\mu)\ln[1+(\mu/\mu')]\},$$

where Q is the product of the above factors and μ and μ' are the mass absorption coefficients for primary and characteristic photons, respectively. A similar argument for a phosphor of finite thickness, where the probability of forward escape p_F is included, yields an expression for p, the total escape probability, which has been integrated numerically in this work using 10 or more sublayers. $(p = p_F + p_B)$.

The variation of p with phosphor thickness is shown in Fig. 1, calculated for an interaction with primary radiation from the isotope Am^{241}. Measurements by Swank and by Kingsley of the output pulse height distribution of CsI phosphors coupled to photomultiplier tubes,[15,16] published in graphical form, can be integrated to obtain p for each phosphor thickness; these are plotted in the figure to demonstrate their agreement with the model.

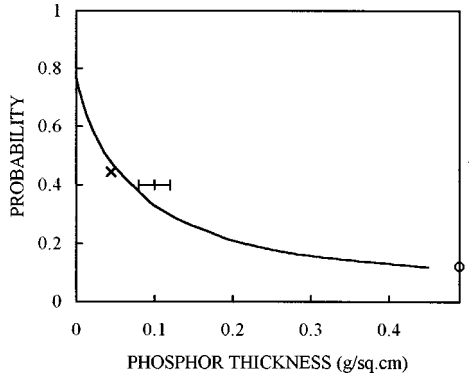

FIG. 1. The probability of $K\alpha/\beta$ photon escape from a CsI phosphor layer per interaction with photons from an Am^{241} source. Data measured by Swank (see Ref. 15) for a thick (○) and for thin (×) crystals, and by Kingsley (see Ref. 16) for a crystal of uncertain thickness (+) are shown.

The variation of p with the energy of the primary radiation for a phosphor thickness of 0.2 g/sq. cm CsI is shown in Fig. 2. Three regions of the energy range can be identified:

(1) Below the K-absorption edge energy of iodine, $K\alpha/\beta$ fluorescence is not possible and no escape occurs. (L-line fluorescence escapes will occur, but the probability is low, the energy loss small, and therefore the influence on m_e and b_e is negligible,)
(2) Between 33.17 and 35.98 keV only iodine is fluoresced; I_K-escape occurs carrying away most of the primary photon energy on these occasions;
(3) Above 35.98 keV both elements are fluoresced. At the lower end of this range a higher value of p is obtained due to strong absorption of primary radiation close to the entry face of the phosphor.

The results of similar calculations for photon escape from Gd_2O_2S at energies above the K-absorption edge of gadolinium at 50.2 keV are also presented in Fig. 2. In practice a higher probability of escape can be expected due to the increased surface area of the powder-phosphor layer in comparison with the solid-film model assumed for this calculation.

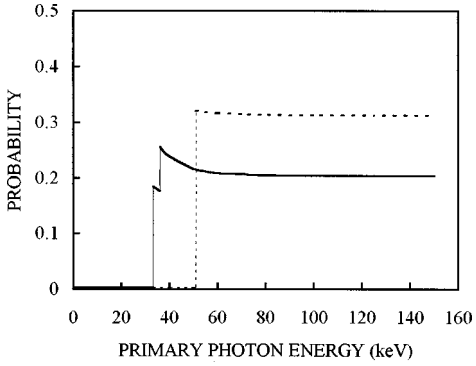

FIG. 2. The probability of characteristic photon escape from a phosphor layer vs primary photon energy. Data are presented for a 0.2 g/sq. cm thick CsI layer (——) and a 0.18 g/sq. cm Gd_2O_2S layer (— — —).

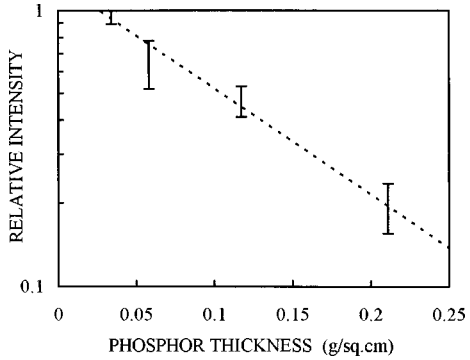

FIG. 3. The intensity of emitted photons transmitted through a layer of Gd_2O_2S powder. The layer is irradiated with a 10 keV electron beam which penetrates less than 1 μm into the phosphor particles.

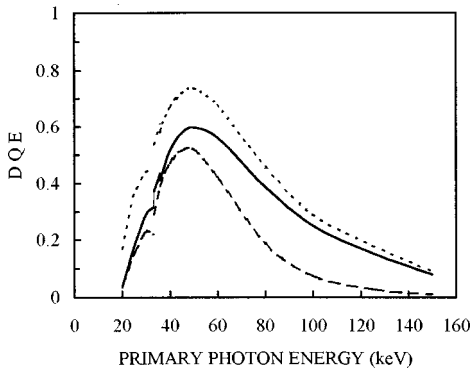

FIG. 4. The detective quantum efficiency of x-ray image intensifiers with CsI input phosphors behind an aluminum/glass vacuum envelope. (——) shows 0.2 g/sq. cm phosphor and (— — —) 0.1 g/sq. cm. (· · · ·) indicates the estimated performance of the thicker phosphor with a 0.25 mm titanium envelope.

The gain and variance of the bimodal escape stage are calculated from the primary photon energy, the deposited energy when the escape process succeeds, and the probabilities of each event. For the gadolinium phosphor this calculation is performed for each sublayer before the summation of Eq. (5).

V. PHOTON ABSORPTION

The probability m_4 that a visible photon generated in the columnar structure will reach the photoemissive layer behind the CsI phosphor is assumed, in the absence of measured data, to be 0.5; errors in this estimate will have little influence on the total variance *B*. In the Gd_2O_2S powder layer, however, strong scattering and absorption of the photons occurs to a degree dependent on the position of the original interaction. As before this is modeled by addition of the output signal and noise from a number of sublayers, calculated for each from the absorption stage ($m_{2,s}$) through to the photoemissive stage before summation.

The transmission of visible photons through a layer of Gd_2O_2S was measured in a scanning electron microscope equipped with a transmitted-electron detector consisting of a phosphor, light pipe, and photomultiplier. The detector phosphor was replaced with Gd_2O_2S layers attached directly to the light pipe with a conducting binder. The phosphor particle size was 5 ± 4 μm. The powder surface was irradiated with a defocused electron beam. The signal outputs are plotted in arbitrary units in Fig. 3 from which the exponential photon absorption coefficient of 9 sq. cm/g can be measured; values of m_4 and b_4 for each sublayer were estimated from this datum. The coefficient will vary with the method of phosphor preparation, the refractive indices of the materials, the acceptance angle of the detector for scattered radiation, etc.

VI. RESULTS AND DISCUSSION

The overall variance *B* and the DQE of an XRII design can be obtained from the estimated gain and variance of each stage in the device. Figures 4 and 5 show the DQE for the various models of intensifier considered here.

Examination of the data leading to Fig. 4 showed that the low value of DQE for low-energy primary photons is due, as expected, to absorption in the input window of the vacuum tube. Above 33.17 keV, the iodine absorption edge energy, the DQE rises discontinuously due to increased absorption in the 0.2 g/sq. cm phosphor layer and the simultaneous onset of I_K-escape events only partially reduces this improvement. Conversely, just above the Cs_K edge at 35.98 keV, though the absorption increases slightly, the escape events from both atomic species predominate and the DQE decreases marginally. Up to 50 keV increased penetration through the vacuum envelope combined with good absorption in the phosphor ($m_2>0.9$) produces higher values of DQE; thereafter, reduced absorption in the CsI results in lower values of DQE. The influence of any proposed change in the physical structure of the tube can be predicted by revision of the quantities in the equations for *B*. For example where the front face of the XRII tube is constructed of a concave 0.25 mm titanium sheet in place of the aluminum/glass envelope, an improvement in DQE is produced particularly in the lower energy region, as shown in the figure. If a thinner layer, 0.1 g/sq. cm CsI, is used with the glass window, the change of DQE at 33.17 keV would be more marked but with only a small loss of performance in the 40–60 keV range.

Figure 5 shows the results of similar calculations for an

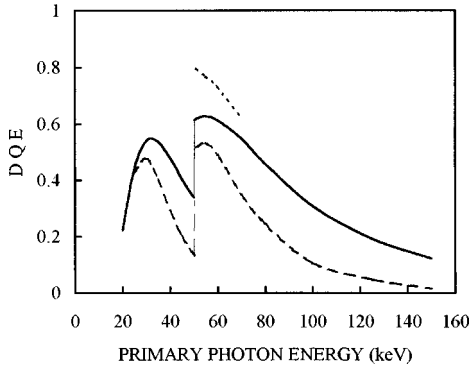

FIG. 5. The detective quantum efficiency of x-ray image intensifiers with gadolinium oxysulphide phosphors and aluminum vacuum envelope. (——) shows the 0.18 g/sq. cm phosphor and (— — —) 0.09 g/sq. cm. The influence of increased primary photon absorption alone (· · · ·) is shown as if the escape mechanism did not exist.

XRII with a Gd_2O_2S input phosphor. While the performance would be similar to the CsI model at about 60 keV the following differences are noted at other energies:

(1) at low energies the aluminum window assumed for the Gd_2O_2S device produces better performance than the glass or titanium windows above;
(2) above 30 keV performance deteriorates due to incomplete absorption in the 0.18 g/sq. cm phosphor despite improved transmission through the input window;
(3) above 50.2 keV performance improves dramatically due to a twofold increase in primary photon absorption in the phosphor. The influence of this factor alone is indicated by the line in the figure ($\cdot\ \cdot\ \cdot$) but, with the onset of the escape mechanism, the improvement is partially negated. If the phosphor layer is reduced to 0.09 g/sq. cm, perhaps to improve spatial resolution, the change of performance at 50.2 keV is emphasized.

Swank[17] considered the absorption and noise in x-ray phosphors alone and calculated their performance in terms of three parameters, the quantum absorption A_Q $\{=m_2\}$, the energy equivalent absorption A_E $\{=m_2.m_e\}$, and the noise equivalent absorption A_N $\{A_N=1/(1+B_n)$ where $B_n=b_2+b_e/m_2\}$. This last parameter is the DQE of the absorption and escape processes alone, all other variances in Eq. (4) here being set to zero. The data by Swank, which were calculated with a more complete model of absorption events, produce results for the escape variance very similar to those calculated here. $[b_e=(A_Q/A_N)-1]$.

The same author discusses the application of the model where the primary photon signal is not monoenergetic and demonstrates that the effective DQE must be obtained from the first- and second-order moments, M_1 and M_2, of the output pulse distribution, averaged over the known or estimated incident x-ray energy distribution. The total relative variance B can be written as M_2'/M_1^2, where the prime indicates the moment about the distribution mean and moment M_1 is the system gain relevant to this analysis (e.g., $m_1.m_2.....m_5$). (The zero-order moment $M_0=1$).

From Eq. (3)

$$M_2=M_1^2+M_2'=M_1^2.(1+B)=M_1^2/\mathrm{DQE}.$$

The average weighted values of the moments, ${}_{\mathrm{av}}M_1$ and ${}_{\mathrm{av}}M_2$, can be calculated and from these the effective DQE is $1/(1+{}_{\mathrm{av}}M_1^2/{}_{\mathrm{av}}M_2)$.

Data published by manufacturers of XRII usually give a ''typical'' value of DQE obtained by comparing the performances of their device and a sodium iodide crystal detector when using Am^{241} radiation. ''The quantum detection efficiency is determined by comparing the measured output SNR of the tube to the measured output SNR of the totally absorbing NaI crystal, which is known to be equal to the input SNR in the case of monochromatic x-ray radiation.''[18] A correction at least for photon escape from the NaI crystal by the method indicated above should be made, however, which would show that the DQE of this totally absorbing device could not exceed 0.97 even if all other stages were perfect. (It is evident that the ''quantum detection efficiency'' here is identical to the DQE of Jones.[5])

ACKNOWLEDGMENTS

The author would like to acknowledge the generous leadership of Dr. J. T. Fourie and Dr. N. R. Comins of this laboratory in, respectively, initiating and publishing a study of secondary electron detectors in electron microscopes which has led to the present work.

[1] P. Shagen, Philos. Trans. R. Soc. London, Ser. A **269**, 233 (1971).
[2] R. K. Swank, Appl. Opt. **12**, 1865 (1973).
[3] W. Shockley and J. R. Pierce, Proc. Inst. Radio Eng. **26**, 321 (1938).
[4] A. Rose, Adv. Electron. Electron Phys. **1**, 131 (1948).
[5] R. C. Jones, Adv. Electron. Electron Phys. **11**, 87 (1959).
[6] E. Breitenberger, Prog. Nucl. Phys. **4**, 56 (1955).
[7] N. R. Comins and J. T. Thirlwall, J. Microsc. **124**, 119 (1981).
[8] U. W. Arndt and D. J. Gilmore, J. Appl. Crystallogr. **12**, 1 (1979).
[9] M. Stanton, W. Phillips, Y. Li, and K. Kalata, J. Appl. Crystallogr. **25**, 638 (1992).
[10] W. Kuhl and J. E. Schrijvers, Medicamundi **22**, 6 (1977).
[11] A. Makovski, *Medical Imaging Systems* (Prentice–Hall, Englewood Cliffs, NJ, 1983), p. 87.
[12] S. J. B. Reed, *Electron Microprobe Analysis* (Cambridge University Press, Cambridge, England, 1975). p. 262.
[13] S. J. B. Reed, in Ref. 12, p. 271.
[14] S. J. B. Reed and N. G. Ware, J. Phys. E **5**, 582 (1972).
[15] R. K. Swank, J. Appl. Phys. **45**, 3673 (1974).
[16] J. D. Kingsley, in *Real-Time Radiologic Imaging: Medical and Industrial Applications*, edited by D. A. Garrett and D. A. Bracher (American Society for Testing Materials, STP716, Philadelphia, 1980), p. 98.
[17] R. K. Swank, J. Appl. Phys. **44**, 4199 (1973).
[18] In ''Technical Specification for GS220 intensifier tube,'' Thomson-CSE, Division Tubes Electroniques, Boulogne-Billancourt, France (1985).